

# GREEN BANK TELESCOPE AND *SWIFT* X-RAY TELESCOPE OBSERVATIONS OF THE GALACTIC CENTER RADIO MAGNETAR SGR J1745–2900

RYAN S. LYNCH<sup>1</sup>, ROBERT F. ARCHIBALD, VICTORIA M. KASPI, AND PAUL SCHOLZ  
Department of Physics, McGill University, 3600 University Street, Montreal, Quebec, H3A 2T8, Canada  
*Draft version December 2, 2014*

## ABSTRACT

We present results from eight months of Green Bank Telescope 8.7-GHz observations and nearly 18 months *Swift* X-ray telescope observations of the radio magnetar SGR J1745–2900, which is located 2′.4 from Sgr A\*. We tracked the magnetar’s radio flux density, polarization properties, pulse profile evolution, rotation, and single-pulse behavior. We identified two main periods of activity in SGR J1745–2900. The first is characterized by approximately 5.5 months of relatively stable evolution in radio flux density, rotation, and profile shape, while in the second these properties varied substantially. Specifically, a third profile component emerged and the radio flux increased on average, but also became more variable. Bright single pulses are visible and are well described by a log-normal energy distribution at low to moderate energies, but with an excess at high energies. The 2–10 keV flux has decayed steadily since the initial X-ray outburst, in contrast with the radio flux. Our timing analysis includes Green Bank Telescope, *Swift*, and *NuSTAR* data. When we include the X-ray data in our analyses, we find that SGR J1745–2900 exhibited a level of timing noise unprecedented in a radio magnetar, though an analysis of only the radio data indicates timing noise at a level similar to that observed in other radio magnetars. We conclude that, while SGR J1745–2900 is similar to other radio magnetars in many regards, it differs by having experienced a period of relative stability in the radio band that now appears to have ended, while the X-ray properties have evolved independently.

*Subject headings:* pulsars: individual (SGR J1745–2900) — stars: magnetars

## 1. INTRODUCTION

Magnetars are neutron stars that display intense short X-ray bursts, X-ray pulsations, and X-ray outbursts that are typically followed by a decaying X-ray flux. The hallmark of magnetar activity is an X-ray luminosity that may exceed the power available from the neutron star’s rotation. Instead, magnetars are believed to be powered by the decay of their enormous internal magnetic fields (Thompson & Duncan 1995, 1996; Thompson et al. 2002; Beloborodov 2009), and the most active magnetars<sup>2</sup> generally have inferred surface dipolar magnetic fields of  $10^{14}$ – $10^{15}$  G, much higher than the  $\sim 10^{12}$  G typical of rotation-powered radio pulsars. Under this interpretation, as the internal magnetic field decays, it stresses the stellar crust, inducing occasional sudden crustal and/or magnetospheric reconfigurations that give rise to the variety of variable X-ray emission.

Pulsed radio emission has been detected from four magnetars thus far (Camilo et al. 2006, 2007a; Levin et al. 2010; Shannon & Johnston 2013). Their radio properties show both similarities and marked differences when compared to those of rotation-powered pulsars. Like all magnetars (e.g. Dib & Kaspi 2014), the four radio magnetars have a high degree of timing noise and experience significant changes in torque (e.g. Camilo et al. 2007c). Both rotation-powered pulsars and radio magnetars exhibit a high degree of linear polarization (Camilo et al.

2007b,a; Kramer et al. 2007; Levin et al. 2012; Shannon & Johnston 2013; Eatough et al. 2013b) and have radio spectra that can be well modeled with a single power law,  $S_\nu \propto \nu^\alpha$ . However, magnetars have shallow or even flat spectra, with  $\alpha$  that may vary significantly with time (e.g. Camilo et al. 2007d), whereas rotation-powered pulsars typically have stable spectra with  $\langle \alpha \rangle \sim -1.6$  (Lorimer et al. 1995). The flux density and pulse profile morphology of some radio magnetars are also highly variable (e.g. Camilo et al. 2007c). This may be due, at least in part, to the emission of erratic, extremely narrow single pulses and very long profile stabilization timescales (Kramer et al. 2007). Single pulse studies of magnetars have not revealed evidence for drifting sub-pulses of the kind sometimes seen in rotation-powered pulsars (Serylak et al. 2009).

The newest of the four known radio magnetars is SGR J1745–2900<sup>3</sup>. The X-ray source was discovered in outburst by Kennea et al. (2013c) using *Swift*. Subsequent observations with the *NuSTAR* X-ray telescope detected pulsations with a spin period  $P = 3.76$  s and  $\dot{P} = 6.5 \times 10^{-12}$  ss<sup>−1</sup>, implying a magnetic field of strength  $B = 1.6 \times 10^{14}$  G, thus confirming the pulsar’s nature as a magnetar (Mori et al. 2013). Radio pulsations at the same period were subsequently detected at several observatories (Shannon & Johnston 2013; Eatough et al. 2013b). SGR J1745–2900 lies only 2′.4 in projection from Sgr A\* (Rea et al. 2013), and its dispersion measure ( $DM = 1778 \pm 3$  pc cm<sup>−3</sup>) implies that the source lies  $< 10$  pc from Sgr A\* itself (Eatough et al. 2013b). Early

[rlynch@physics.mcgill.ca](mailto:rlynch@physics.mcgill.ca)

<sup>1</sup> Department of Physics and Astronomy, West Virginia University, PO Box 6315, Morgantown, WV 26506, USA

<sup>2</sup> For an up-to-date list, see the McGill magnetar catalog at <http://www.physics.mcgill.ca/~pulsar/magnetar/main.html> (Olausen & Kaspi 2014).

<sup>3</sup> Olausen & Kaspi (2014) also refer to this source as MG J1745–2900.

radio observations have measured a flat spectrum and high degree of polarized emission for SGR J1745–2900, much like in other radio magnetars (Eatough et al. 2013a; Shannon & Johnston 2013).

Here, we report on the results from an observing campaign of SGR J1745–2900 using the Robert C. Byrd Green Bank Telescope (GBT), supplemented with data from the *Swift* X-ray Telescope (XRT) and *NuSTAR* telescope. We tracked the evolution of the spin, radio flux density, polarization, and profile morphology of the pulsar at 8.7 GHz, and have also analyzed properties of its single pulses. XRT was used to measure the 2–10 keV flux. We first provide relevant background on the magnetar’s behavior in §2. In §3 we describe our observational set-up and data reduction. Our analysis and results are presented in §4, and discussed in more detail in §5.

## 2. OVERVIEW OF RADIO AND X-RAY BEHAVIOR

Before we discuss our results in detail, we provide some context by highlighting some of the radio and X-ray properties of SGR J1745–2900 reported elsewhere. Radio pulse profiles obtained shortly after the magnetar was first detected had a single Gaussian component across a wide range of frequencies, including  $\sim 8$ –9 GHz (Shannon & Johnston 2013; Spitler et al. 2014), though there appears to be visual hints of a second profile component emerging in some of the profiles presented by Eatough et al. (2013b). The early reported flux densities near 9 GHz varied but were of order  $\sim 1$  mJy.

After the initial outburst, the X-ray flux of SGR J1745–2900 began to decay. The *Swift* Burst Alert Telescope (BAT) detected short bursts on MJDs 56407 (25 April 2013; Kennea et al. 2013d), 56450 (7 June 2013; Kennea et al. 2013a), and 56509 (5 August 2013; Kennea et al. 2013b). Despite this, the overall flux decay continued. Kaspi et al. (2014) suggested that the burst on MJD 56450 may have been accompanied by a change in spin-down ( $\dot{f}$ ), though there was no discontinuity in spin frequency. This behavior was not consistent with a glitch or anti-glitch, though timing noise could not be ruled out.

Yusef-Zadeh et al. (2014) observed SGR J1745–2900 on 25 February 2014 (MJD 56713) at 44 GHz with the Very Large Array and measured a flux density that was  $\sim 20$  times higher than an upper limit obtained in August 2011. Simultaneous *Chandra* observations showed no evidence of a corresponding increase in X-ray flux (Rea et al. 2014). We observed SGR J1745–2900 31 days prior to and 13 days after this 44-GHz flux density increase (on MJDs 56682 and 56726, respectively). As discussed below, our data provide evidence that SGR J1745–2900 underwent a change in flux density, pulse profile morphology, and possibly rotational parameters sometime between the above two observations, changing from a fairly stable state to a more erratic radio state. We will refer to the stable state (covering MJDs 56515–56682) and erratic state (covering MJDs 56726–56845) throughout. We will discuss the extent with which we can associate this state change with the 44-GHz radio brightening in §5.

## 3. OBSERVATIONS AND DATA REDUCTION

### 3.1. Green Bank Telescope

We observed SGR J1745–2900 on 33 epochs. We used an approximately weekly cadence from 11 August 2014 through 25 January 2014<sup>4</sup>, during which integration times averaged about 30 minutes. Because SGR J1745–2900 was fairly stable over this period, we planned on switching to a monthly cadence with two hour integrations starting in February 2014. However, after two monthly monitoring sessions, it became apparent that the magnetar increased in variability. Therefore, we re-allocated our time to allow for more frequent but shorter, 30 minute, observations, though scheduling constraints prevented us from restarting weekly sessions.

We used the X-band receiver system of the GBT at a center frequency  $\nu_c = 8.7$  GHz and with an instantaneous bandwidth of  $\Delta\nu = 800$  MHz, recording dual circular polarizations. The data were recorded with the the Green Bank Ultimate Pulsar Processing Instrument, using 512 frequency channels and a sampling time of  $\delta t = 163.84 \mu\text{s}$ . At the beginning of each observing session we took on and off-source scans of a standard flux calibrator while firing the GBT pulsed noise diode. We initially used 3C353 as a flux standard, but after noticing anomalies in the flux densities we calculated, we switched to using 3C286 on and after 12 May 2014 (see §4.1 for a detailed discussion of our reported flux density measurements). We observed the noise diode again at the position of SGR J1745–2900 before observing the magnetar, and used these data for calibration purposes.

The data were folded modulo the rotational period of SGR J1745–2900, using 1024 bins in pulse phase and sub-integrations with a duration of one rotation, thus preserving information on individual single pulses. Radio frequency interference (RFI) was usually minimal, but when present we excised it manually by explicitly removing contaminated frequency channels and sub-integrations. We also removed  $\sim 2.5\%$  from the top and bottom of the frequency band due to roll-off in the receiver sensitivity. This was usually sufficient for obtaining integrated pulse profiles with few artifacts, but on certain epochs significant fluctuations in the off-pulse region were evident (as an example, see the profile from MJD 56677 in Figure 1). The effect is usually (though not exclusively) associated with observations that occurred at elevation angles below  $\sim 10^\circ$ , and we believe that they are primarily caused by changes in atmospheric opacity. To ensure that the fluctuations are not intrinsic to SGR J1745–2900, we folded the data at a period randomly drawn from a uniform distribution on an interval  $P \pm 0.5$  s, where  $P = 3.76$  s is the spin period of the magnetar. This effectively allowed us to sample the period space around the magnetar while avoiding bias in the chosen period. As expected, similar fluctuations were readily apparent when folding at the randomly selected period, demonstrating that they are extrinsic to SGR J1745–2900.

After folding and RFI excision, the total, linearly, and circularly polarized flux densities were calibrated using standard routines from the PSRCHIVE software package (Hotan et al. 2004). On and off-source observations of the standard flux calibrator were used to measure the

<sup>4</sup> No observations were possible from 4–18 October 2013 because GBT operations were suspended due the U.S. Federal Government shutdown.

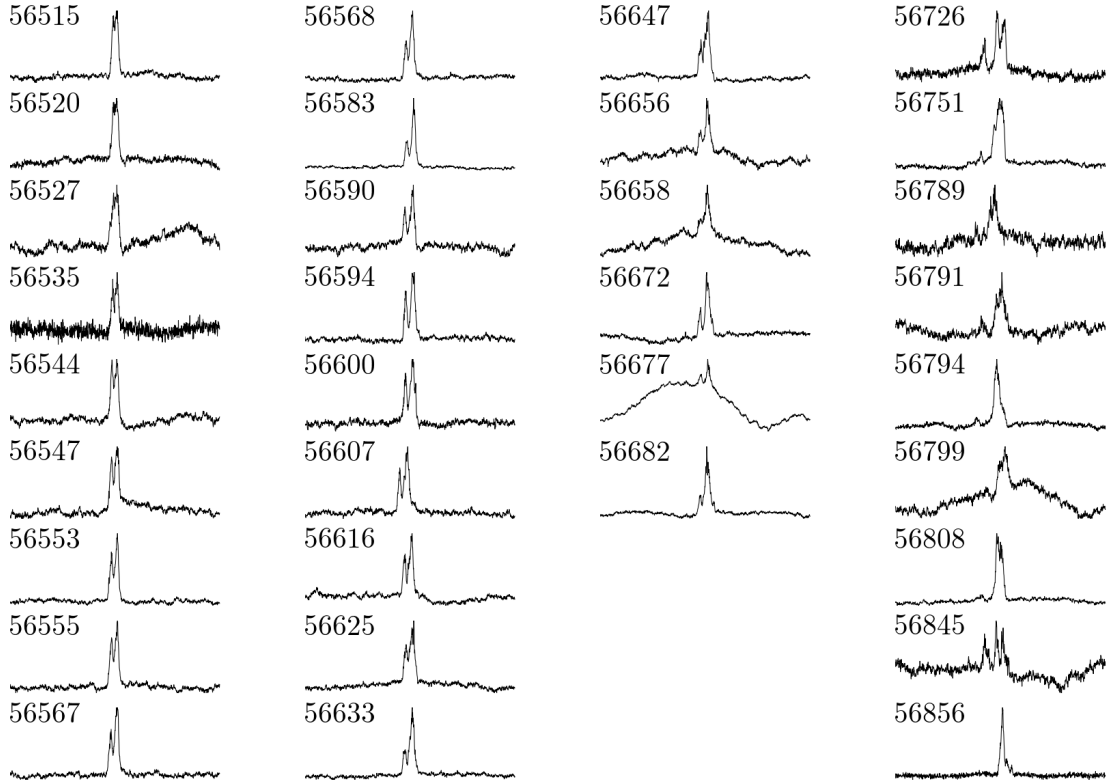


**Figure 1.** Integrated 8.7-GHz pulse profiles of SGR J1745–2900 at each of our observing epochs, which are indicated by MJD. For clarity, profiles are centered and scaled to have the same peak amplitude. As described in the text, baseline fluctuations that we attribute to changes in atmospheric opacity are evident at certain epochs, and are not intrinsic to SGR J1745–2900. Up to MJD 56682 (first three columns), the profile shape was fairly stable, exhibiting a clear double peaked structure. Changes in the relative amplitude of the two peaks are most likely due to the pulse-to-pulse variability, given the relatively small number of rotations observed at each epoch, which prevents the profile from fully stabilizing. Starting with MJD 56726 (fourth column), the profile became more variable, often showing a third component.

absolute flux density of the pulsed noise diode, and this in turn was used to calibrate the total and polarized flux density of SGR J1745–2900. We corrected for Faraday rotation by searching over a range of rotation measures (RMs, again using PSRCRIVE standard tools), from  $-2 \times 10^5 \leq \text{RM} \leq 0 \text{ rad m}^{-2}$ , de-rotating our data at the RM that maximized the linearly polarized flux density. All subsequent analyses were performed on these calibrated, RM-corrected data unless otherwise noted.

### 3.2. *Swift* XRT

In order to characterize the X-ray flux evolution of SGR J1745–2900, we analyzed 416 *Swift* XRT observations of the source obtained between MJDs 56407 and 56956 as part of the Galactic center monitoring program (Degenaar et al. 2013). Observations were typically 1-ks long and occurred nearly daily, except between MJDs 56599 and 56690, when the source was in Sun-constraint. A total of  $\sim 438$  ks of data were analyzed.

The XRT (Burrows et al. 2005) is a Wolter-I telescope with an *XMM-Newton* EPIC-MOS CCD22 detector, sensitive in the 0.5–10 keV range. For all the observations presented here, the XRT was operated in Photon Counting (PC) mode, which has a time resolution of 2.5 s. We obtained Level-1 data products from the HEASARC *Swift* archive, reduced them using the *xrt-pipeline* standard reduction script, and reduced them to

the Solar system barycenter them using the *Chandra* position (Rea et al. 2013) of SGR J1745–2900 using HEASOFT v6.16. Individual exposure maps, spectra, and ancillary response files were created for each orbit and then summed.

## 4. ANALYSIS

### 4.1. Radio Flux and Polarization Properties

We began the process of measuring the mean flux density,  $S_\nu$ , of SGR J1745–2900 by systematically identifying the on-pulse region at each epoch. This was done by identifying the profile bins to both the left and right of the profile peak at which the flux density reached the root-mean-square (RMS) level of the integrated profile as a whole. This gave us a rough idea of the on-pulse and off-pulse bins. We iterated this procedure using the RMS of the updated off-pulse region until the results converged. The baseline fluctuations described in §3 may bias this procedure in two ways—by raising the off-pulse RMS and by making the on-pulse region appear broader than it actually is. We attempted to mitigate this by fitting a third order polynomial to the integrated profile (but using only the off-pulse region) and subtracting it to flatten the baseline. We used this approach to determine the on-pulse region, but used the original, unflattened profile to calculate  $S_\nu$ .

We found that, when using 3C353 as flux calibrator,

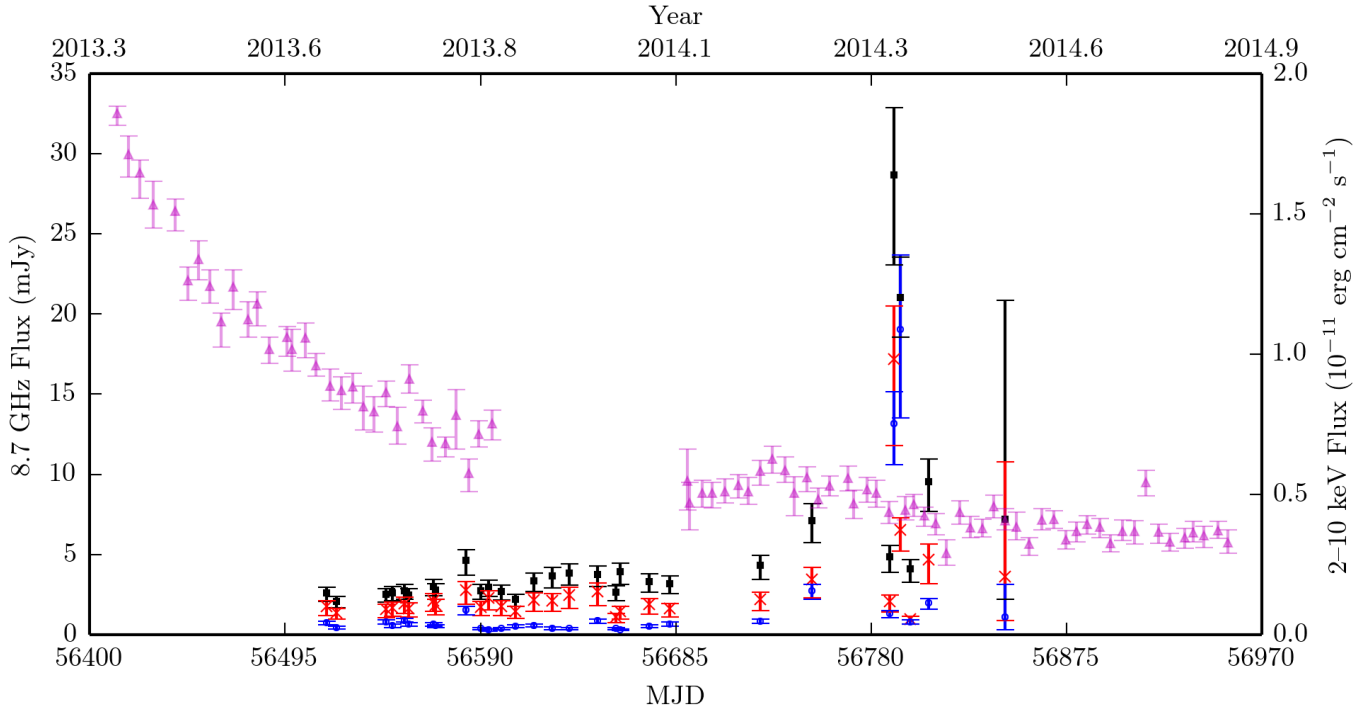


**Figure 2.** The period averaged 8.7-GHz flux density and 2–10 keV flux of SGR J1745–2900. The squares (black), crosses (red), and circles (blue) indicate total, linearly polarized, and circularly polarized radio flux density, respectively. X-ray fluxes are indicated by triangles (magenta). Within the uncertainties in our measurements, the radio flux was relatively stable up to MJD 56682, with a mean of  $\sim 3$  mJy. After MJD 56726, the flux was more erratic. The X-ray flux has decayed steadily since the initial outburst and is well modeled by a double exponential function (see text for parameters). The moderate X-ray flux increase around MJD 56731 is associated with another source. The flare on MJD 56910 is most likely associated with Sgr A\*.

our calculated 8.7-GHz flux densities were consistently a factor of  $\sim 10$ – $20$  higher than those reported by [Shannon & Johnston \(2013\)](#) and [Eatough et al. \(2013b\)](#) at similar frequencies. To confirm this discrepancy we observed both 3C353 and 3C286 on the same date, and calibrated our data from that date independently using both sources. The data calibrated using 3C286 were in rough agreement with the two previous reports of  $S_{8.7 \text{ GHz}}$  (which we note were obtained independently from each other with different telescopes), while the data calibrated using 3C353 were a factor of several higher. From this, we concluded that 3C353 is not a reliable flux standard at these frequencies. We subsequently used only 3C286 for flux calibration, observing it at a total of five epochs, though a hardware error made one of these unusable for flux calibration. To measure the flux density at all of our observing epochs, we independently calibrated all of our data using the four reliable 3C286 observations. This resulted in four separate flux measurements at each of our 33 observing epochs, although three epochs had to be discarded from the flux density analysis because of malfunctions of the noise diode. Even though we used the same flux standard, there was still scatter among these four flux density values. The flux density we report here is the mean of these and the uncertainties represent the minimum and maximum of the four independent flux density values. Our experience highlights the inherent difficulty of obtaining reliable absolute flux density measurements and can hopefully serve as a cautionary tale to other observers.

The radio flux density is shown in 2 (along with the X-ray flux), while the fractional polarization is shown

in 3. During the previously identified stable state (see §2), the flux density of SGR J1745–2900 was nearly constant, with a mean  $S_{8.7 \text{ GHz}} \approx 3.0$  mJy and a standard deviation of 0.62 mJy between measurements. For comparison, the mean uncertainty in our measurements of  $S_{8.7 \text{ GHz}}$  during this state was  $^{+0.6}_{-0.4}$  mJy. Like other authors ([Shannon & Johnston 2013](#); [Eatough et al. 2013b](#)), we also measure a high degree of linear polarization. The mean linear polarization fraction in the stable state was

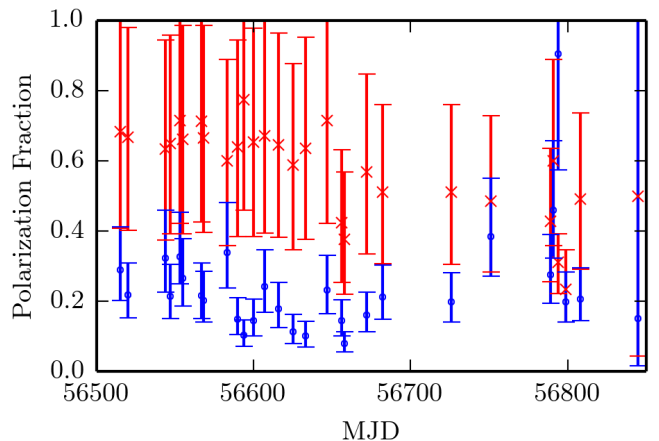


**Figure 3.** The fraction of linearly and circular polarization. The symbols are the same as in the top panel. During the stable state the linear polarization fraction was relatively constant at  $\sim 0.6$ , though the uncertainties are large. The circular polarization fraction was typically  $\sim 0.2$ . During the erratic state, the circular polarization fraction increased to a mean of  $\sim 0.4$  while the linear polarization fraction decreased to a mean of  $\sim 0.4$ .



0.6 with a standard deviation of 0.09. The circular polarization was much smaller at 0.2 and with a standard deviation of 0.08.

During the erratic state, the flux of SGR J1745–2900 was both higher and more variable. The mean flux was  $S_{8.7\text{ GHz}} \approx 11$  mJy but with a standard deviation of 8.5 mJy and mean uncertainties of  $^{+3.1}_{-2.4}$  mJy. Not only was the standard deviation in  $S_{8.7\text{ GHz}}$  a substantial fraction of the mean (0.78), it was much larger than the uncertainties. The circular polarization fraction increased slightly, with a mean of 0.4 and standard deviation of 0.2, while the linear polarization fraction decreased to a mean of 0.4 with standard deviation of 0.1.

#### 4.2. X-ray Flux

To investigate the X-ray flux and spectral behavior, we extracted a circular region centered on SGR J1745–2900 and with a diameter of a  $20''$ , chosen to match the half-power diameter of the XRT at 4 keV. An annulus of inner radius  $20''$ , and outer radius  $60''$  centered on the source was used to extract background spectra. This is the same background region used by Kennea et al. (2013c). As the angular distance between SGR J1745–2900 and Sgr A\* is  $2''.4 \pm 0''.3$ , we note that our source region also contains Sgr A\*. We summed the spectra in five-day intervals, and grouped them to have a minimum of three counts per bin. Photoelectric absorption was modeled using XSPEC `tbabs`, with abundances from Wilms et al. (2000), and photoelectric cross-sections from Verner et al. (1996). We then fit the spectra to a photoelectrically absorbed black body using the “lstat” statistic. The spectra were fit jointly, with a single neutral hydrogen column density ( $N_{\text{H}}$ ) and temperature ( $kT$ ), allowing only the black body normalization to vary for each spectrum. A variable  $kT$  was not statistically warranted. This gave best-fit values of  $N_{\text{H}} = (12.1 \pm 0.3) \times 10^{22} \text{ cm}^{-2}$  and  $kT = 1.00 \pm 0.01 \text{ keV}$  ( $\chi^2 = 8585$  for 8917 degrees of freedom, or `lstat` = 8620.68). These values of  $N_{\text{H}}$  and  $kT$  are consistent with those reported by Kennea et al. (2013c).

The evolution of 2–10 keV flux is shown alongside  $S_{8.7\text{ GHz}}$  in Figure 2. The flux decay is reasonably well fit ( $\chi^2 = 92.6$  for 76 degrees of freedom) by the sum of two exponential decay functions:

$$F = \left[ (1.00 \pm 0.06) e^{-(t-t_0)/(55 \pm 7 \text{ d})} + (0.98 \pm 0.07) e^{-(t-t_0)/(500 \pm 41 \text{ d})} \right] \times 10^{-11} \text{ erg cm}^{-2} \text{ s}^{-1}, \quad (1)$$

where  $t_0 = 56406$  is the the peak of the outburst. There is a small flux increase around MJD 56731 due to nearby source leaking into the extraction region, and is not related to the magnetar. There is also a flare evident on MJD 56910 that is likely due to Sgr A\* (Degenaar et al. 2014). We see no significant change in the 2–10 keV flux coincident with onset of erratic radio behavior.

#### 4.3. Radio Profile Shape Evolution

Integrated radio pulse profiles of SGR J1745–2900 are shown in Figure 1 for each of our observing epochs. The profile underwent significant changes over the course of

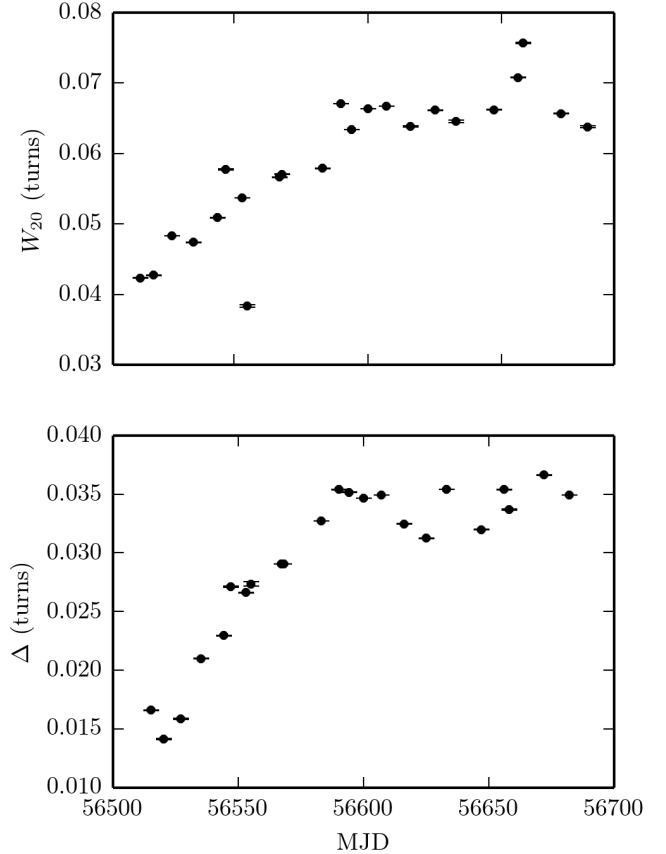


**Figure 4.** Full width at 20% of peak flux ( $W_{20}$ ) and peak-to-peak separation ( $\Delta$ ) as a function of time for SGR J1745–2900. Only the stable state is shown. Error bars indicate the  $1\text{-}\sigma$  confidence intervals. There is a linear increase in both parameters between MJDs 56544 and 56594.

our observations. In our earliest data, the profile appeared double peaked, although the two peaks were not always clearly separated prior to MJD 56544. During this period the profile was well fit using a two-component Gaussian model. The most obvious changes in the profile were variations in the relative amplitude of the two Gaussian components from epoch to epoch, which may be due to pulse-to-pulse variability. However, there were also more subtle, long-term changes in the profile. We characterized these by measuring the full width at 20% peak amplitude ( $W_{20}$ ) and the separation between the two peaks in the profile ( $\Delta$ ). Each quantity was measured by fitting an analytic, two-component Gaussian model to the on-pulse region. The peak amplitude was measured by finding the global maximum of the fit, and  $W_{20}$  was found using a bisection method to determine the phase at which the model crossed the 20% flux level on both the leading and trailing sides of the pulse. To measure  $\Delta$  we simply calculated the pulse phase corresponding to each profile peak.

Uncertainties were quantified following the method outlined by Ferdman et al. (2013). We randomly removed half the profile bins from the on-pulse region, fit a new Gaussian model, and re-calculated the shape parameters as above. We performed 1000 independent Monte Carlo trials and calculated the mean values and the 68.27% (i.e.,  $1\text{-}\sigma$ ) confidence intervals for each parameter from the resulting distributions. The results of

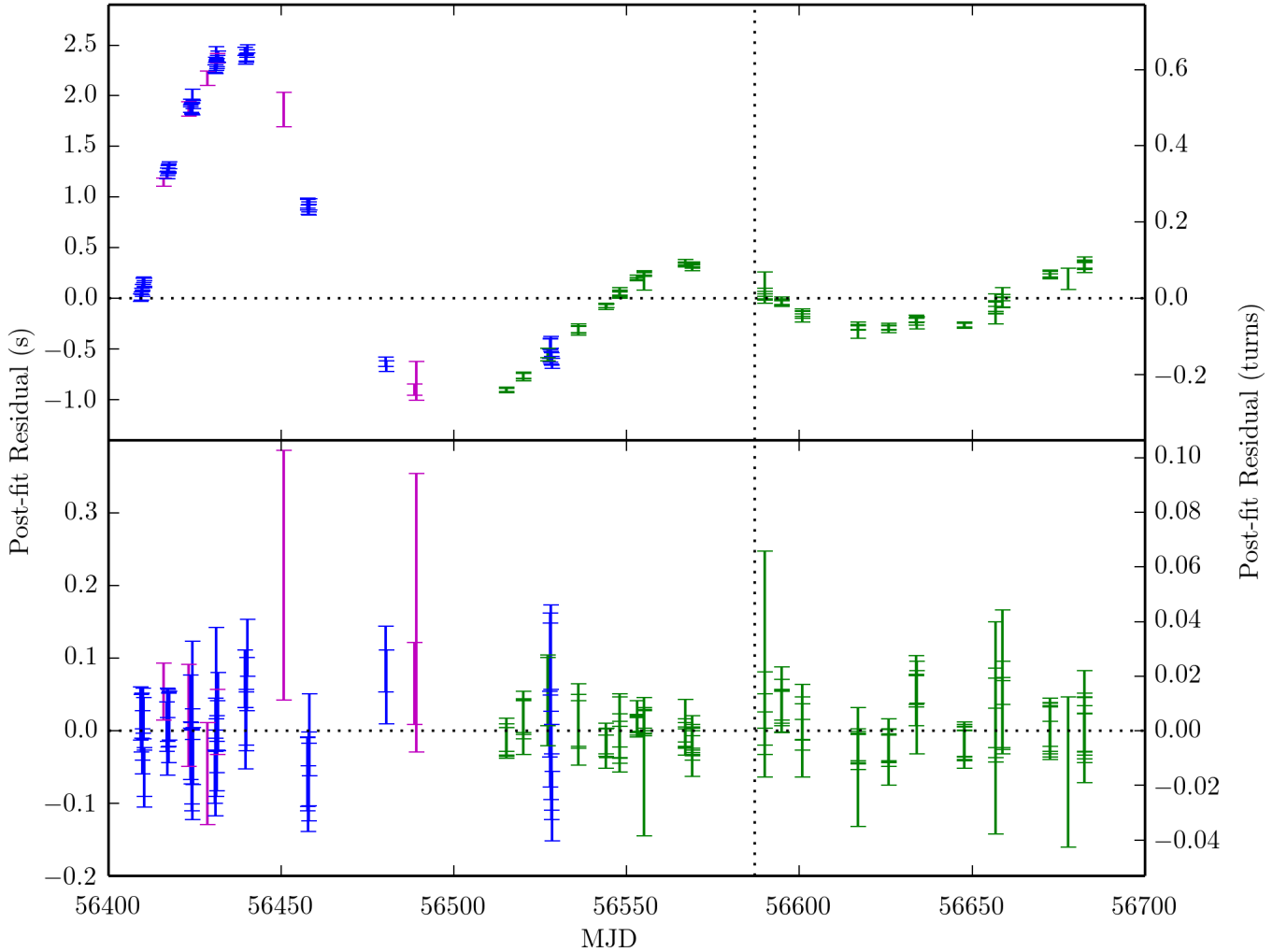


**Figure 5.** Post-fit timing residuals as a function of MJD. Only data from the stable state are shown here because we could not unambiguously phase connect data from the erratic state. TOAs from our GBT observations (green) are shown along with those previously published by Kaspi et al. (2014) from *Swift* (magenta) and *NuSTAR*. The vertical dotted line indicates the reference epoch used in our timing model. The radio and X-ray TOAs are independently phase connected, with an arbitrary phase offset applied to align the two data sets. *Top*: The residual structure fitting only for  $f$ ,  $\dot{f}$ ,  $\ddot{f}$ , and  $f^{(3)}$ . The effects of timing noise are clearly evident. *Bottom*: The results of fitting for twelve frequency derivatives presented. Note the much smaller horizontal scale.

this analysis are shown in Figure 4.

There was an obvious increase in both  $W_{20}$  and  $\Delta$  between MJDs 56544 and 56594. Although there is significant scatter compared to our uncertainties, we fit a linear trend to the data over this span and find a rate of change in both  $W_{20}$  of and  $\Delta$  of  $0.08 \pm 0.04^\circ \text{ day}^{-1}$ . A linear fit to the data between MJDs 56594 and 56682 is consistent with no steady change in either quantity. Because both  $W_{20}$  and  $\Delta$  changed by the same amount, the increase in pulse width can be attributed solely to an increase in the peak separation.

With the onset of the erratic state, the profile changed dramatically. Due to these large variations we did not calculate  $W_{20}$  and  $\Delta$  for this period. A third component emerged separated by  $\sim 0.1$  turns from the centroid of the persistent double-peaked main components. Between MJDs 56726 and 56856 the relative amplitude of this third component varied significantly, from nearly equal to the two other components to only barely above the noise level. Furthermore, the primary profile component varied between the previously described double-peaked

form and a single, broad shape.

#### 4.4. Pulsar Timing

We began the timing analysis of the radio data by fitting a noise-free Gaussian template to a high signal-to-noise (S/N) integrated profile. We used the same template for data obtained during the stable state, i.e. when the magnetar had only two profile components. As noted above, the profile varied from epoch to epoch during this time, which could introduce a bias to our TOAs. However, the profile variations were subtle, with the total change in  $\Delta$  amounting to only  $\sim 0.02$  turns, which is of the same order as the RMS scatter in our timing residuals and much less than the accumulated phase drift due to timing noise. As such, we are confident that the use of a single template is sufficient for this span of observations. The onset of the erratic state made timing difficult, as discussed below. In all cases, pulse times of arrival (TOAs) were calculated via Fourier domain cross-correlation (Taylor 1992) of the templates with the calibrated and RM corrected pulse profiles at each observing

epoch. We usually obtained one topocentric TOA per 100 rotations of the magnetar, summing all frequency channels.

We were also able to include previously published TOAs obtained with *Swift* and *NuSTAR* (see [Kaspi et al. 2014](#) for a description of the data set and how these TOAs were obtained). The XRT PC-mode data used to measure 2–10 keV flux lacked the time resolution to measure pulsed emission, hence no TOAs are available from this dataset. We allow for an arbitrary phase shift between the X-ray TOAs and those obtained with the GBT, which can absorb differences in the profiles, phase offsets between the radio and X-ray emission, DM delays, instrumental shifts, etc. Hence, we cannot determine an absolute phase offset between the radio and X-ray pulses.

TEMPO was used to fit a phase-coherent spin-down model to the radio and X-ray TOAs, making use of the DE421 Solar System ephemeris for barycentering and the TT(BIPM12) clock correction chain. We held the coordinates of SGR J1745–2900 fixed at those reported by [Rea et al. \(2013\)](#) and the DM fixed at the value reported by [Eatough et al. \(2013b\)](#), and hence only fitted for the rotational frequency,  $f$ , and its derivatives.

We were able to unambiguously phase connect all radio TOAs during the stable state. We found that a simple spin-down model accounting only for  $f$  and  $\dot{f}$  was insufficient for describing the long-term rotational behavior of SGR J1745–2900 (see the top panel of Figure 5) up to MJD 56682. This is common among magnetars, which exhibit a large degree of timing noise and typically require many higher-order frequency derivatives to accurately model their rotational phase. We used twelve frequency derivatives, the maximum allowed by TEMPO, but we caution that this model is not predictive, and is only used to whiten the residuals. Our final solution is presented in Table 1. Fully whitened post-fit residuals are shown in the bottom panel of Figure 5. The reduced  $\chi^2$  of our timing solution was large even after fitting all twelve frequency derivatives. To obtain a reduced  $\chi^2$  of one, we multiplied the individual TOA errors by a constant error factor,  $\epsilon = \sqrt{\chi^2/\text{d.o.f.}} = 6.4$ .

Although we could not phase connect the radio and X-ray TOAs, we were able to find single a solution that adequately fit this entire data set, allowing only for the phase offset between the two frequencies. [Kaspi et al. \(2014\)](#) reported a possible abrupt change in  $\dot{f}$  around MJD 56450, which suggestively was coincident to an X-ray burst. Our results indicate that the suggested change in  $\dot{f}$  is consistent with timing noise, and that a second distinct rotational ephemeris is not needed after MJD 56450. It is common to characterize timing noise as the cumulative contribution over the span of observations of the cubic term in the Taylor expansion of rotational phase (e.g. [Arzoumanian et al. 1994](#)):

$$\Delta_t(t) = \left( \frac{1}{6f} |\ddot{f}| t^3 \right) \quad (2)$$

where  $t$  is the duration of timing observations. We find  $\Delta_t = 864$  s (230 cycles) over a time span of approximately 273 days. This is significantly larger than in other radio magnetars:  $\sim 120$  s (22 cycles) over 277 days for XTE J1810–197 ([Camilo et al. 2007c](#)),  $\sim 124$  s (60

**Table 1**  
Timing Parameters of SGR J1745–2900

Data, Statistics, & Assumptions	
Data Span (MJD) .....	56409–56682
$N_{\text{TOA}}$ .....	165
Residual RMS (ms) .....	25.6
Solar System Ephemeris ...	DE421
Clock Correction Procedure	TT(BIPM12)
Fixed Quantities	
Right Ascension (J2000) ...	17 <sup>h</sup> 45 <sup>m</sup> 40 <sup>s</sup> .169
Declination (J2000) .....	–29°00′29″.84
DM (pc cm <sup>–3</sup> ) .....	1778
Reference Epoch (MJD) ...	56587.0
Measured Quantities	
$f$ (Hz) .....	0.2656936554(12)
$\dot{f}$ (Hz s <sup>–1</sup> ) .....	$-1.2399(15) \times 10^{-12}$
$\ddot{f}$ (Hz s <sup>–2</sup> ) .....	$-1.047(13) \times 10^{-19}$
$f^{(3)}$ (Hz s <sup>–3</sup> ) .....	$6.7(1.9) \times 10^{-27}$
$f^{(4)}$ (Hz s <sup>–4</sup> ) .....	$3.74(18) \times 10^{-32}$
$f^{(5)}$ (Hz s <sup>–5</sup> ) .....	$-7.1(2.0) \times 10^{-39}$
$f^{(6)}$ (Hz s <sup>–6</sup> ) .....	$-3.90(26) \times 10^{-44}$
$f^{(7)}$ (Hz s <sup>–7</sup> ) .....	$-5.0(1.4) \times 10^{-51}$
$f^{(8)}$ (Hz s <sup>–8</sup> ) .....	$3.34(30) \times 10^{-56}$
$f^{(9)}$ (Hz s <sup>–9</sup> ) .....	$1.83(11) \times 10^{-62}$
$f^{(10)}$ (Hz s <sup>–10</sup> ) .....	$-1.37(17) \times 10^{-68}$
$f^{(11)}$ (Hz s <sup>–11</sup> ) .....	$-1.71(15) \times 10^{-74}$
$f^{(12)}$ (Hz s <sup>–12</sup> ) .....	$-5.05(43) \times 10^{-81}$
Derived Quantities	
$B_s$ (G) .....	$2.6018(16) \times 10^{14}$
$\dot{E}$ (erg s <sup>–1</sup> ) .....	$1.3005(16) \times 10^{34}$
$\tau_c$ (yr) .....	3395.2(4.1)

**Note.** — Numbers in parentheses represent 1- $\sigma$  uncertainties in the last digits as determined by TEMPO, scaled such that the reduced  $\chi^2$  equals one.

cycles) over 6 months for 1E 1547.0–5408 ([Camilo et al. 2008a](#)), and  $\sim 1080$  s (250 cycles) over 20 months for PSR J1622–4950 ([Levin et al. 2012](#)). However, if we do not include the X-ray TOAs and instead restrict our analysis to the period covered by our phase-connected GBT observations, we find  $\Delta_t = 140$  s (37 cycles) over a time span of approximately 167 days. This is closer to the level of timing noise observed in other radio magnetars.

The onset of the erratic state and the accompanying profile changes required a change in our timing analysis, as the simple standard template we used during the stable state was no longer adequate. We explored three options for obtaining TOAs: using the same three-component Gaussian template for all epochs, using a different Gaussian template for each epoch, and using a template based on the folded profiles at each epoch, but with noise removed using a wavelet smoothing algorithm. In the latter two cases, we attempted to align the different templates using the peak of the leading profile component as our reference point. We obtained TOAs using each method and attempted to extend the solution obtained during the stable state, but could not unambiguously maintain phase connection. We also tried to use a subset of TOAs from epochs just before the onset of the erratic state to establish a new solution without

the need for many higher order frequency derivatives, and then to extend this simplified solution into the erratic state. Again, we could not unambiguously phase connect the data. Finally, we attempted to form a solution from only the TOAs obtained during the erratic state, as the magnetar could have experienced a glitch or other sudden change in rotational parameters, but we still could not obtain a phase-connected solution. We are therefore unable to provide a precise timing solution for the erratic state. The implications of this are discussed in §5.

#### 4.5. Single Pulses

##### 4.5.1. Energy distribution

SGR J1745–2900 emits bright single pulses during most rotations. We analyzed the energy distribution, sub-pulse structure, and emission phase of the pulses. We recorded the peak flux in the on-pulse region during each rotation, but discarded a rotation if the peak flux never reached  $\geq 3$  times the off-pulse noise level. The peak fluxes at each epoch were normalized by the mean peak flux at that epoch. A histogram of these normalized fluxes is shown in Figure 6. The distribution of peak fluxes roughly follows a log-normal distribution with a logarithmic mean  $\mu \approx -0.163$  and standard deviation  $\sigma \approx 0.548$ . There appears to be a high-energy tail to the observed distribution, however. The log-normal approximation underestimates the observed number of pulses at fluxes  $F \gtrsim 2.5\langle F \rangle$ , and especially at  $F \gtrsim 4\langle F \rangle$ . We note, though, that only 416 pulses out of 11428 (about 3.6%) have  $F \geq 2.5\langle F \rangle$ . Levin et al. (2012) found that the single pulses of PSR J1622–4950 also followed a log-normal distribution. A careful analysis of single pulses from XTE J1810–197 by Serylak et al. (2009) found a more complex distribution of single pulse energies, with emission sometimes best described by a combination of a power law and log-normal distribution because of the presence of a high-energy tail. In this regard, SGR J1745–2900 seems similar to XTE J1810–197.

##### 4.5.2. Drifting Sub-pulses

We employed the 2D fluctuation spectrum method of Edwards & Stappers (2002) to search for and characterize any potential drifting sub-pulses. This method relies on a power spectrum of the 2D Fourier transform of pulse flux as a function of pulse phase and pulse number, i.e.

$$S(u, v) = \left| \frac{1}{K} \sum_{j=0}^{n_{\text{bins}}-1} \sum_{k=0}^{n_{\text{pulses}}-1} F(j, k) e^{-2\pi i(uj+vk)} \right|^2, \quad (3)$$

where  $K = n_{\text{bins}} \times n_{\text{pulses}}$  is a normalization factor (Lorimer & Kramer 2005). The signature of drifting sub-pulses is harmonic structure in  $S(u, v)$ , from which we can determine the characteristic spacing between sub-pulses and the period with which sub-pulses drift in phase.

The baseline fluctuations described in §3 caused significant red noise in  $u$ . There was sometimes an increase in power in  $v$ , but this was seen even when we only analyzed the off-pulse region (either in full or a randomly selected subset). As such, we attribute it to an artifact of the data processing. We see no evidence for drifting sub-pulses in SGR J1745–2900.

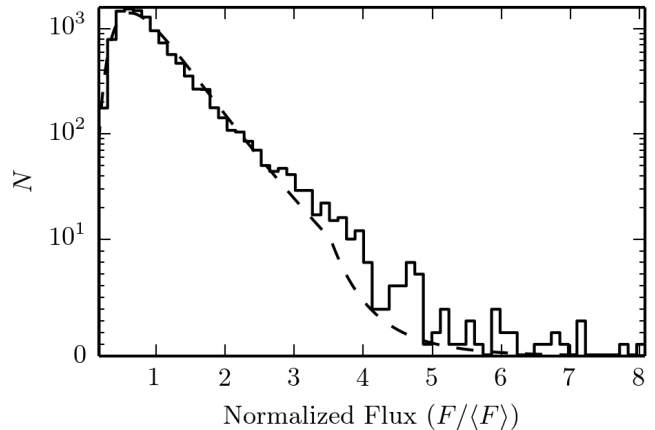


**Figure 6.** A histogram of peak single-pulse flux, normalized by the mean peak flux at that epoch. The dashed line shows the best-fit log-normal distribution, as described in the text. The presence of a high-energy tail is clearly visible above four times the mean flux. Note that the ordinate scaling changes from linear to logarithmic at values above 10.

##### 4.6. Search for Off-pulse Radio Burst Emission

Some magnetars are observed to emit extremely bright X-ray bursts lasting  $\sim$  few ms. These bursts are sporadic and can occur at phases not typically associated with the on-pulse region. The magnetic reconnection model proposed by Lyutikov (2002) makes a clear prediction that such X-ray bursts should be accompanied by simultaneous radio bursts with very high fluxes. This model is particularly interesting in light of the recent discovery of a population of extremely bright, short duration radio bursts of apparently cosmological origin (Lorimer et al. 2007; Thornton et al. 2013). Unfortunately, we were unable to obtain simultaneous X-ray/radio observations of SGR J1745–2900, but we can still search for radio bursts that occur outside of the on-pulse region which, if detected, would be highly suggestive. For this analysis, we used tools in the PRESTO<sup>5</sup> software suite (Ransom et al. 2002) that do not require identifying an on-pulse region. We de-dispersed the raw GBT data using an RFI mask generated by PRESTO at both the DM of the magnetar ( $1778 \text{ pc cm}^{-3}$ ) and at  $\text{DM} = 0 \text{ pc cm}^{-3}$ , so that we could reject any remaining RFI. We then conducted a blind search for single pulses by match-filtering the data with boxcar functions of various widths, ranging from  $163.84 \mu\text{s}$  (our native resolution) to  $\sim 5 \text{ ms}$ . We then calculated the corresponding pulse phase of all single pulses with  $\text{S/N} \geq 5$ , rejecting pulses that also appeared in the un-dispersed time series. No pulses were detected outside of the main pulse window. Of course, this does not rule out the Lyutikov (2002) model, since it may simply be the case that no X-ray bursts occurred during our observations.

## 5. DISCUSSION

SGR J1745–2900 is similar to other radio magnetars in many regards. It has a high degree of linear polarization, with a lower but significant fraction of circular polarization. It exhibits a high degree of timing noise. Its single pulse energy distribution is similar to that of XTE J1810–197. However, during the stable state it

<sup>5</sup> <http://www.cv.nrao.edu/~sransom/presto/>



showed a level of radio flux density and profile stability not often seen in radio magnetars.

During the stable state, we observed a steady evolution in the separation between the two profile peaks. Prior to the start of our GBT observations, the profile was apparently single-peaked. The growing separation between the peaks that we observed may suggest that the profile evolved smoothly from single to double peaked. However, the extended periods of minimal change in peak separation that we observed indicate that any such smooth change did not occur steadily. The emergence of the third profile component marked the onset of the erratic state, but as noted in §4.3, there are hints of a widely separated component in some of the profiles presented by Eatough et al. (2013b). A joint analysis of both data sets could link this with the third component we observed. If this were the case it would raise the question of why the component remained dormant for many months before abruptly reappearing.

Unlike the radio flux density, the X-ray flux has decayed mostly steadily since the initial outburst, although some short bursts have been detected with the *Swift* BAT (see §2). For comparison, the radio magnetar XTE J1810–197 faded in both the radio and X-ray bands following its discovery (Camilo et al. 2007c). The X-ray flux of 1E 1547–5408 decayed steadily following an outburst, while the radio flux density varied (Camilo et al. 2008b). PSR J1622–4950 was discovered via its radio emission while in an X-ray quiescent state, with no X-ray outbursts detected in archival data as far back as four years prior to its radio discovery (Levin et al. 2010). This suggests that the radio emission in PSR J1622–4950 is long-lived and not related to its X-ray emission, and in this regard appears similar to SGR J1745–2900.

What caused SGR J1745–2900 to move into the erratic state? The change in mean flux and profile morphology suggest a significant reconfiguration of the magnetosphere. It would be useful to know if this was associated with a glitch or sudden change in spin-down, as is sometimes correlated with profile changes in other radio pulsars (Lyne et al. 2010). Unfortunately, our inability to maintain phase connection during this state prevents us from making such a definitive statement. We can speculate on the reasons for losing phase connection. One possibility is that the profile changes introduced too much uncertainty into the definition of a fiducial point in the profile to maintain phase connection. It is also possible that the gap between our observations was simply too large to maintain phase-coherence, given the uncertainties in the rotational parameters. We cannot rule this out, but we do note that the timing model presented by Kaspi et al. (2014) was accurate enough to maintain phase connection throughout the entire stable state, even before making any adjustments to the solution based on the radio data. Timing noise was clearly evident, but phase connection was maintained. The duration of the stable state was far greater than the  $\sim 30$  day gap between the observations over which we lost phase connection, and introducing an artificial  $\sim 30$  day gap in our data does not result in a loss of phase connection during the stable state. On the other hand, based on our analysis of timing noise presented in §4.4, SGR J1745–2900 exhibited a degree of timing noise unprecedented in radio magnetars when we included the time span covered

by *NuSTAR* and *Swift* timing observations. This timing noise was apparently large enough that it could also be interpreted as a sudden change in  $\dot{f}$ , possibly associated with an X-ray burst (Kaspi et al. 2014). Thus, there is precedent for timing noise in SGR J1745–2900 sufficient to introduce ambiguities in phase connected timing solutions. It is interesting to note, however, the coincidence between the radio variability and our inability to phase-connect, with both beginning roughly  $\sim 300$  days after the initial outburst. If our timing difficulties are not due to the gap or to the varying pulse profile, then this is reminiscent of behavior seen in magnetar 1E 1048.1–5937, in which, now three times, delayed torque variability followed, after a  $\sim 100$  day decay, an X-ray outburst (Arcibald et al. submitted). In the latter case, radio emission is not seen, possibly due to unfavorable beaming. We speculate that we could therefore be seeing similar behavior in SGR J1745–2900, but with the additional radio diagnostic. Under this scenario we would expect a relatively stable X-ray pulse profile for SGR J1745–2900 during the radio-variable phase. Unfortunately, we cannot verify this due to the low XRT PC-mode time resolution.

It is tempting to speculate that the increase in 44-GHz flux density (Yusef-Zadeh et al. 2014) is connected with the emergence of the third profile component. Unfortunately, the gap between the high frequency brightening and our closest observations prevent us from associating these events definitively. The measured flux of both observations that were taken closest to the 44-GHz brightening is not anomalously high, but we do see an eventual increase in  $S_{8.7\text{ GHz}}$ . This suggests that the 44-GHz brightening was not long-lived, but may be associated with greater variability in flux overall.

## 6. CONCLUSIONS

We observed the magnetar SGR J1745–2900 for eleven months using the GBT, measuring its radio flux density, pulse profile shape, single-pulse behavior, and timing parameters. We have also analyzed publicly available *Swift* XRT data from the initial outburst of the magnetar, tracking its X-ray flux and spectral evolution. We find that for the first 5.5 months of our GBT observations, the radio flux density and pulse profile remained relatively stable, with a slow increase in the pulse width and separation between two profile peaks. This is in contrast to the three other radio magnetars, which were all highly variable in the radio band. During this time, the magnetar exhibited a high degree of timing noise but did not otherwise experience any anomalous rotational behavior. After this stable period, SGR J1745–2900 entered an erratic state marked by a higher and more variable radio flux density and significant changes in the radio pulse profile from epoch to epoch. We were unable to maintain phase connection, but can only speculate as to the causes. The onset of this erratic state occurred within two weeks of a short-lived increase in radio density at 44 GHz measured with the VLA (Yusef-Zadeh et al. 2014). The X-ray flux of SGR J1745–2900 has steadily decayed since the initial outburst, and did not deviate from this trend at any point during the time span covered by our GBT observations, including during the erratic radio state. We conclude that whatever caused the erratic radio state is decoupled from the X-ray emis-

sion.

The authors wish to thank Paul Demorest for invaluable assistance in processing the GBT data, and for helping to track down and correct some instrumental and hardware errors. The GBT is operated by the National Radio Astronomy Observatory, which is a facility of the National Science Foundation operated under cooperative agreement by Associated Universities, Inc. We acknowledge the use of public data from the *Swift* data archive. This research made use of the XRT Data Analysis Software (XRTDAS) developed under the responsibility of the ASI Science Data Center (ASDC, Italy). The *NuSTAR* mission is a project led by the California Institute of Technology, managed by the Jet Propulsion Laboratory, and funded by the National Aeronautics and Space Administration. This research made use of the *NuSTAR* Data Analysis Software (NuSTARDAS) jointly developed by ASDC and the California Institute of Technology. V. Kaspi receives support from an NSERC Discovery Grant and Accelerator Supplement, from the Centre de Recherche en Astrophysique du Québec, an R. Howard Webster Foundation Fellowship from the Canadian Institute for Advanced Study, the Canada Research Chairs Program, and the Lorne Trottier Chair in Astrophysics and Cosmology. R. Archibald receives support from a Walter C. Sumner Memorial Fellowship.

#### REFERENCES

- Arzoumanian, Z., Nice, D. J., Taylor, J. H., & Thorsett, S. E. 1994, *ApJ*, 422, 671
- Beloborodov, A. M. 2009, *ApJ*, 703, 1044
- Burrows, D. N., Hill, J. E., Nousek, J. A., et al. 2005, *Space Sci. Rev.*, 120, 165
- Camilo, F., Ransom, S. M., Halpern, J. P., & Reynolds, J. 2007a, *ApJ*, 666, L93
- Camilo, F., Ransom, S. M., Halpern, J. P., et al. 2006, *Nature*, 442, 892
- Camilo, F., Reynolds, J., Johnston, S., Halpern, J. P., & Ransom, S. M. 2008a, *ApJ*, 679, 681
- . 2008b, *ApJ*, 679, 681
- Camilo, F., Reynolds, J., Johnston, S., et al. 2007b, *ApJ*, 659, L37
- Camilo, F., Cognard, I., Ransom, S. M., et al. 2007c, *ApJ*, 663, 497
- Camilo, F., Ransom, S. M., Peñalver, J., et al. 2007d, *ApJ*, 669, 561
- Degenaar, N., Miller, J. M., Kennea, J., et al. 2013, *ApJ*, 769, 155
- Degenaar, N., Reynolds, M., Miller, J., et al. 2014, *The Astronomer's Telegram*, 6458, 1
- Dib, R., & Kaspi, V. M. 2014, *ApJ*, 784, 37
- Eatough, R., Karuppusamy, R., Champion, D., et al. 2013a, *The Astronomer's Telegram*, 5058, 1
- Eatough, R. P., Falcke, H., Karuppusamy, R., et al. 2013b, *Nature*, 501, 391
- Edwards, R. T., & Stappers, B. W. 2002, *A&A*, 393, 733
- Ferdman, R. D., Stairs, I. H., Kramer, M., et al. 2013, *ApJ*, 767, 85
- Hotan, A. W., van Straten, W., & Manchester, R. N. 2004, *PASA*, 21, 302
- Kaspi, V. M., Archibald, R. F., Bhalerao, V., et al. 2014, *ArXiv e-prints*, arXiv:1403.5344
- Kennea, J. A., Burrows, D. N., Cummings, J., et al. 2013a, *The Astronomer's Telegram*, 5124, 1
- . 2013b, *The Astronomer's Telegram*, 5254, 1
- Kennea, J. A., Burrows, D. N., Kouveliotou, C., et al. 2013c, *ApJ*, 770, L24
- Kennea, J. A., Krimm, H., Barthelmy, S., et al. 2013d, *The Astronomer's Telegram*, 5009, 1
- Kramer, M., Stappers, B. W., Jessner, A., Lyne, A. G., & Jordan, C. A. 2007, *MNRAS*, 377, 107
- Levin, L., Bailes, M., Bates, S., et al. 2010, *ApJ*, 721, L33
- Levin, L., Bailes, M., Bates, S. D., et al. 2012, *MNRAS*, 422, 2489
- Lorimer, D. R., Bailes, M., McLaughlin, M. A., Narkevic, D. J., & Crawford, F. 2007, *Science*, 318, 777
- Lorimer, D. R., & Kramer, M. 2005, *Handbook of Pulsar Astronomy*, ed. R. Ellis, J. Huchra, S. Kahn, G. Rieke, & P. B. Stetson (Cambridge University Press)
- Lorimer, D. R., Yates, J. A., Lyne, A. G., & Gould, D. M. 1995, *MNRAS*, 273, 411
- Lyne, A., Hobbs, G., Kramer, M., Stairs, I., & Stappers, B. 2010, *Science*, 329, 408
- Lyutikov, M. 2002, *ApJ*, 580, L65
- Mori, K., Gotthelf, E. V., Zhang, S., et al. 2013, *ApJ*, 770, L23
- Olausen, S. A., & Kaspi, V. M. 2014, *ApJS*, 212, 6
- Ransom, S. M., Eikenberry, S. S., & Middleditch, J. 2002, *AJ*, 124, 1788
- Rea, N., Haggard, D., Baganoff, F., et al. 2014, *The Astronomer's Telegram*, 5922, 1
- Rea, N., Esposito, P., Pons, J. A., et al. 2013, *ApJ*, 775, L34
- Serylak, M., Stappers, B. W., Weltevrede, P., et al. 2009, *MNRAS*, 394, 295
- Shannon, R. M., & Johnston, S. 2013, *MNRAS*, 435, L29
- Spitler, L. G., Lee, K. J., Eatough, R. P., et al. 2014, *ApJ*, 780, L3
- Taylor, J. H. 1992, *Royal Society of London Philosophical Transactions Series A*, 341, 117
- Thompson, C., & Duncan, R. C. 1995, *MNRAS*, 275, 255
- . 1996, *ApJ*, 473, 322
- Thompson, C., Lyutikov, M., & Kulkarni, S. R. 2002, *ApJ*, 574, 332
- Thornton, D., Stappers, B., Bailes, M., et al. 2013, *Science*, 341, 53
- Verner, D. A., Ferland, G. J., Korista, K. T., & Yakovlev, D. G. 1996, *ApJ*, 465, 487
- Wilms, J., Allen, A., & McCray, R. 2000, *ApJ*, 542, 914
- Yusef-Zadeh, F., Roberts, D., Heinke, C., et al. 2014, *The Astronomer's Telegram*, 6064